Geophys. J. Int. (1994) **116,** 252–266

A two-year comparison between the French and Canadian superconducting gravimeter data

Jacques Hinderer,[1] David Crossley[2] and Hui Xu[2]

[1] *Institut de Physique du Globe, 5 rue René Descartes, 67084 Strasbourg Cedex, France*
[2] *Geophysics Laboratory, McGill University, 3450 University Street, Montreal, Quebec* H3A 2A7, *Canada*

Accepted 1993 April 30. Received 1993 March 29; in original form 1992 November 27

SUMMARY

This study is devoted to a preliminary comparison of the gravity records provided by two geographically well-separated superconducting gravimeters over a common two-year observing period. The data sets are processed for the first time following exactly the same numerical steps. After a brief description of the observed gravity and pressure signals, we perform a classical least-squares fit to tides, taking into account a single coefficient for the effect of the local barometric pressure fluctuations and a second-order polynomial approximation for the instrumental drift. The results show a totally different drift behaviour between the two instruments. The time fluctuation of the resulting residual gravity signals is shown, as well as the corresponding power spectral density. In particular, we provide detailed statistics on the spectral content of the residual gravity signals. In a subsequent step, we first high-pass filter the observed gravity and pressure signals and then apply an automatic method to detect and remove obvious spikes. A new least-squares fit then provides new residual gravity signals, the power spectral density of which is reduced in all frequency bands, especially in the subtidal band. We finally provide cross-spectral estimates of these two residual gravity sets indicating a further reduction in the power spectral density level.

Key words: gravity.

INTRODUCTION

One of the first analyses of a long record obtained from a superconducting gravimeter (SCG) was performed 15 years ago on an instrument located at Pinon Flat (California). This study, using a 1.5 yr recording, was mainly devoted to tidal research (Warburton & Goodkind 1978), as well as to an investigation of ocean loading (Warburton, Beaumont & Goodkink 1975) and atmospheric loading (Warburton & Goodkind 1977) effects. Later on, in 1980, two other SCG were installed in Europe, one in Brussels (Belgium) and one in Bad Homburg (Germany), this second station being located only 320 km away from the first. Numerous studies were conducted on the data sets obtained with these two instruments dealing with important issues such as the resonance effect between the Nearly Diurnal Free Wobble (NDFW) and tidal gravity, as well as the search for geophysical signals originating in the Earth's fluid core (Ducarme, Van Ruymbeke & Poitevin, 1986; Melchior & Ducarme 1986; Zürn, Rydelek & Richter 1986; Melchior *et al.* 1988; Aldridge & Lumb 1987; Zürn *et al.* 1987; Aldridge, Lumb & Anderson 1988; Mansinha, Smylie & Sutherland 1990) or signals induced by the polar motion (Richter 1983, 1986; Richter & Zürn, 1986). Such studies are possible due to the low drift and high sensitivity of superconducting gravimeters which is of the order of one ngal (one part in 10^{12} of the Earth's surface gravity). More recently, additional SCGs were installed in Wuhan (China), Strasbourg (France), Cantley (Canada) and four in Japan. In particular, the Strasbourg instrument was used in a calibration study involving a parallel registration with an absolute gravity meter (Hinderer *et al.* 1991c) and in detailed investigation of non-tidal periodicities in the gravity signal (Florsch *et al.* 1991). After these investigations which involved individual stations, the first stacking was done using simultaneously the Brussels and Bad Homburg SCGs by Neuberg, Hinderer & Zürn (1987) in order to retrieve from the inversion of diurnal tidal gravimetric factors the NDFW parameters. Finally, very recently, the first stack using several superconducting gravity meters (two records from Brussels (1982–86, 1987–91), one from Bad Homburg (1986–88) and one from Strasbourg (1987–91)) was done by Smylie *et al.* (1993) in order to investigate common periodic or quasi-periodic gravity signals in the subtidal

frequency band (below 8 hr period); only a few lines were found above the noise level and none strictly above the 95 per cent confidence interval. Nevertheless, the coincidence of three spectral lines in the observations with theoretical conjectures (Smylie *et al.* 1993) was the basis of the recent claim by Smylie (1992) for the identification of the translational triplet of the solid inner core (Slichter eigenmodes). This claim has not gone unchallenged (Crossley, Rochester & Peng 1992). Unfortunately, the three European instruments are located too close to each other to dismiss definitely any regional systematic effect of oceanic or atmospheric origin for instance. Moreover the stack by Smylie *et al.* (1993) uses residual gravity signals which have been processed to remove (with a least-squares fitting procedure) lunisolar tides, local air-pressure contribution and long-term instrumental drift, differently for each data set. Additionally, the raw gravity signals from different stations are recorded, digitized and pre-processed in significantly different ways.

Our primary aim in this study is to process, using identical procedures, the gravity records provided by the French and Canadian superconducting gravimeters over a common observing period of two years (14 December 1989–13 December 1991). The two meters are located at comparable latitudes (48.62°N and 45.58°N for the French station near Strasbourg and the Canadian station at Cantley, Quebec, respectively), although the difference in longitude reaches more than 80° (7.68°E and 75.80°W, respectively). Moreover, to make the comparison even more meaningful, we process the two data sets by following exactly the same numerical steps starting from the original 2 s sampling rate of the digitized gravity signal.

CONTENT OF THE GRAVITY SIGNAL

Before starting the comparison of the data sets recorded at the two stations, we briefly recall here the basic content of the observed gravity signal (e.g. Florsch *et al.* 1991):

$$\Delta g(t) = s_0(t) + d(t) + b(t) + n(t) + e(t), \quad (1)$$

$s_0(t)$ is the lunisolar tidal gravity which is the dominant contribution to the observed signal, reaching typically a few hundreds of μgal ($1\ \mu\text{gal} = 10^{-8}\ \text{m s}^{-2}$) and is classically expressed as a function of the theoretical tidal potential in the following way (e.g. Melchior 1983):

$$s_0(t) = \sum_{i=1}^{n} \delta_i \cos \kappa_i \sum_{j=1}^{m_i} A_{ij} \cos(\omega_{ij} t + \phi_{ij}) - \sum_{i=1}^{n} \delta_i \sin \kappa_i \sum_{j=1}^{m_i} A_{ij} \sin(\omega_{ij} t + \phi_{ij}), \quad (2)$$

where n is the number of wave groups and m_i the number of individual tidal waves in the group i, each of them being completely defined by an amplitude A_{ij}, an angular velocity ω_{ij} and a phase (with respect to a fixed reference epoch) ϕ_{ij}. Moreover, to take into account the elastogravitational deformation of the Earth in response to tidal forcing (e.g. Hinderer & Legros 1989; Hinderer *et al.* 1991b), a set of gravimetric amplitude and phase factors (δ_i, κ_i) is introduced for each group i. One of the main purposes of tidal research is of course to compare the observed gravimetric factors to those theoretically predicted (see e.g. Dehant & Ducarme 1987; Dehant & Zschau 1989). In eq. (1), $d(t)$ is the instrumental long-term drift, which is usually approximated for superconducting gravimeters by a low-order polynomial or an exponential function (Richter 1983, 1986). $b(t)$ represents gravity signals associated with physical processes such as atmospheric, ocean or ice loading, changes in the water table level, rainfall, tilt of the building, as well as geophysical signals such as changes in the Earth's rotation, rotational and translational eigenmodes of the solid inner core and gravity-inertial modes of the outer core. $n(t)$ expresses an additive coloured noise, microseismic background noise for example. $e(t)$ is a signal containing disturbances to the instrument, either man-made (e.g. during the transfer of liquid helium) or caused by earthquakes. The property of these disturbances is that they are very short in time (typically a few hours) and appear either like spikes in a long record (see Florsch *et al.* 1991), when the gravity excursion comes back to its original value, or offsets when there is a net change in the mean gravity level.

COMPARATIVE ANALYSIS OF UNFILTERED GRAVITY AND PRESSURE SIGNALS

Raw gravity

The observing period in this study provides 730 days of continuous common gravity and local barometric pressure signals. The original digitizing rate of the gravity feedback voltage (which keeps the superconducting levitating sphere in the same position) is one value every 2 s for the Strasbourg instrument and one value every s (of which only every second sample is kept) for the Cantley meter. An analogue low-pass pre-filter (cut-off period of 50 s and 36 db per octave attenuation) is used in Strasbourg to prevent aliasing before digitization. The same pre-filter was used in Cantley at the beginning but, in February 1990, a modified low-pass analogue filter (with a cut-off period of about 5 s and 20 db attenuation at the Nyquist frequency 0.5 Hz) was installed. Both analogue filters are flat to the corner frequencies but induce small phase shifts in the response which have to be corrected later. The signal is decimated to one point every 5 min by applying to the 2 s data a numerical low-pass symmetrical filter running over 20 min designed in Strasbourg by R. Lecolazet (it is the result of convolving four averaging filters of different lengths). It is necessary to pre-process the 5 min gravity signal in order to remove the major disturbances $e(t)$ of instrumental origin (helium transfer, instrumental maintenance), due to data acquisition problems or caused by earthquakes. In a very traditional way, we have edited our 5 min raw gravity samples by locating by eye these disturbances and filling the related gaps with a local synthetic tide using a set of known (from a previous tidal fit at each station) gravimetric amplitude and phase factors for the major tidal groups. A new decimation with a second low-pass filter running over 24 hr and having a cut-off period of 3 hr is then performed which provides hourly samples of gravity and local pressure. The frequency response of this filter is shown on the top part of Fig. 1. Both gravimeters have been calibrated against absolute gravity meters and the expected calibration

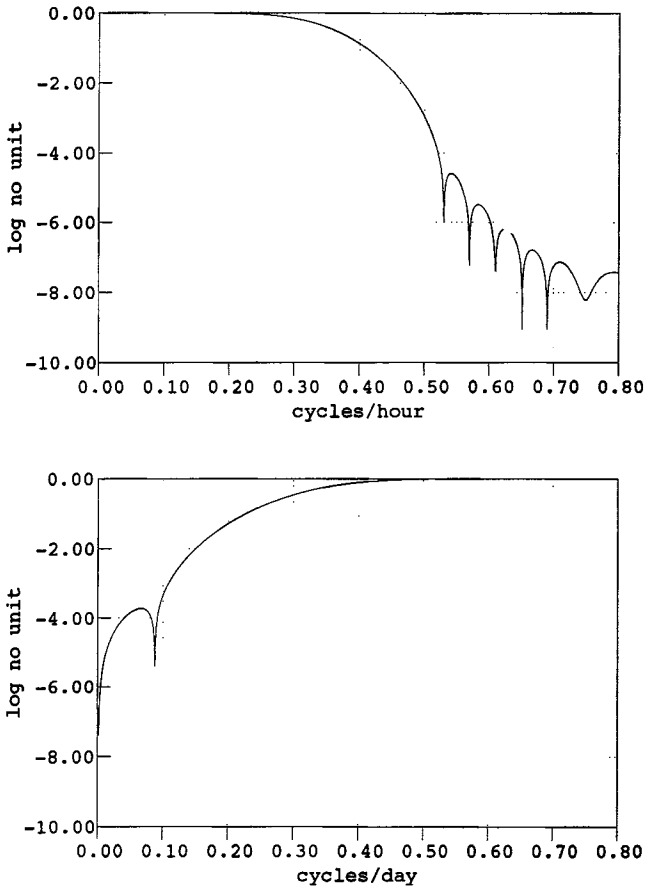

Figure 1. Spectral response of the low-pass decimation filter (top) and of the high-pass filter (bottom) used in this study. The low-pass filter which decimates the 5 min gravity and pressure samples to hourly values has a nominal cut-off period of 3 hr and runs over one day (289 coefficients). The high-pass filter has a nominal cut-off period of three days and its length slightly exceeds two weeks (361 hourly coefficients).

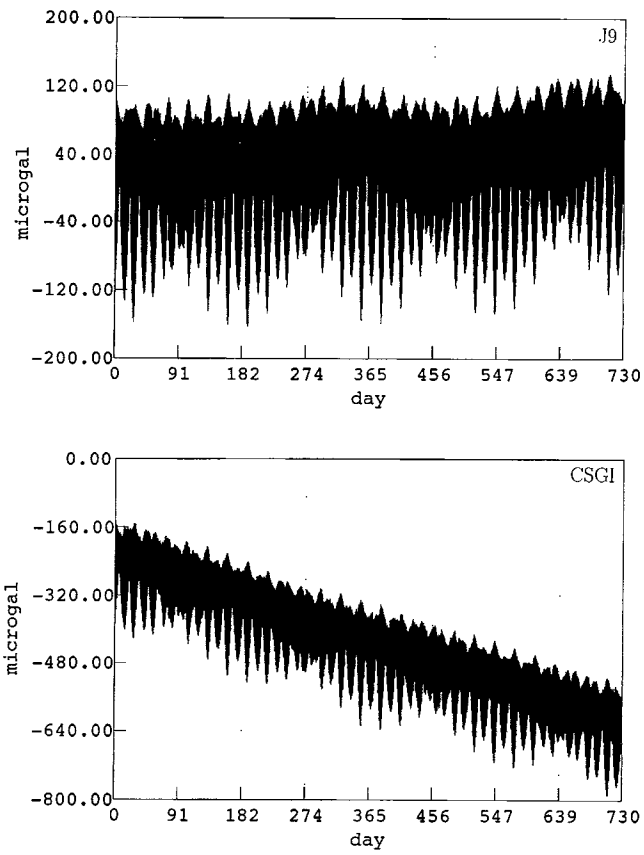

Figure 2. Time fluctuations of the raw observed gravity signals for the Strasbourg station J9 (top) and the Cantley station CSGI (bottom).

accuracy is of the order of 1 per cent (Hinderer *et al.* 1991c; Bower *et al.* 1991).

The time fluctuations of the raw gravity are shown in Fig. 2 (the reference levels are arbitrary); as will always be the case hereafter, the top curve is for the Strasbourg station (called J9) and the bottom curve for Cantley (called CSGI, Canadian Superconducting Gravimeter Installation). The tidal gravity changes reach about 200 μgal and show the multiple long-period (e.g. fortnightly and semi-annual) modulation of the major semi-diurnal and diurnal tides. The drift behaviour of the instruments is totally different; while there is a slight increasing gravity for the Strasbourg meter, that for Cantley exhibits a large almost linear drift towards negative gravity values. The exact cause of the unusual CSGI drift and its sign is still not very well known and is partly attributed to physical properties of the superconducting parts (sphere and coils) operated in the liquid helium (Warburton 1991, personal communication). The histograms of the raw gravity signals are not worth showing because they merely represent the superimposition of long-term drift and tides. In fact, the histogram of a theoretical tide would exhibit a large negative skewness because of the non-symmetrical character of the zenithal dependence ($3\cos^2 z - 1$, where z is the zenithal distance of the Moon or Sun) of the largest degree 2 lunisolar tides (Melchior 1983).

We have also computed the power spectral densities (PSD) (in μgal^2 per cycle per hour (cph)) of the gravity signals; they are shown on a logarithmic scale in Fig. 3. The PSD are smoothed periodograms. We applied a cosine bell data taper (with a length ratio of 1/10 with respect to the total length of the data, meaning that 90 per cent of the data are undisturbed) to the signals which are then padded and Fourier transformed. Failure to taper the data can easily mask the effect of the low-pass decimation filter, which occurs at frequencies between 0.3 and 0.5 cph (the Nyquist frequency for hourly samples).

In order to reduce the scatter on the PSD plots, we also convolved the unsmoothed spectra with a Parzen spectral window (truncated at the first zero in frequency) running over 11 frequency samples; this window was chosen because of its superior characteristics, compared with the box-car window, in side lobe reduction in the lag domain (see e.g. Jenkins & Watts 1969).

We clearly see the tidal harmonic lines (long-period, diurnal, semi-diurnal and ter-diurnal) emerging from a power-law decrease in the gravity signal as a function of the frequency f (from 0 to 0.5 cph); of course, the rapid attenuation starting at 0.3 cph is caused by the decimation filter. The signal is a combination of instrumental drift and disturbances, atmospheric loading, and other physical signals such as hydrogeological changes which are

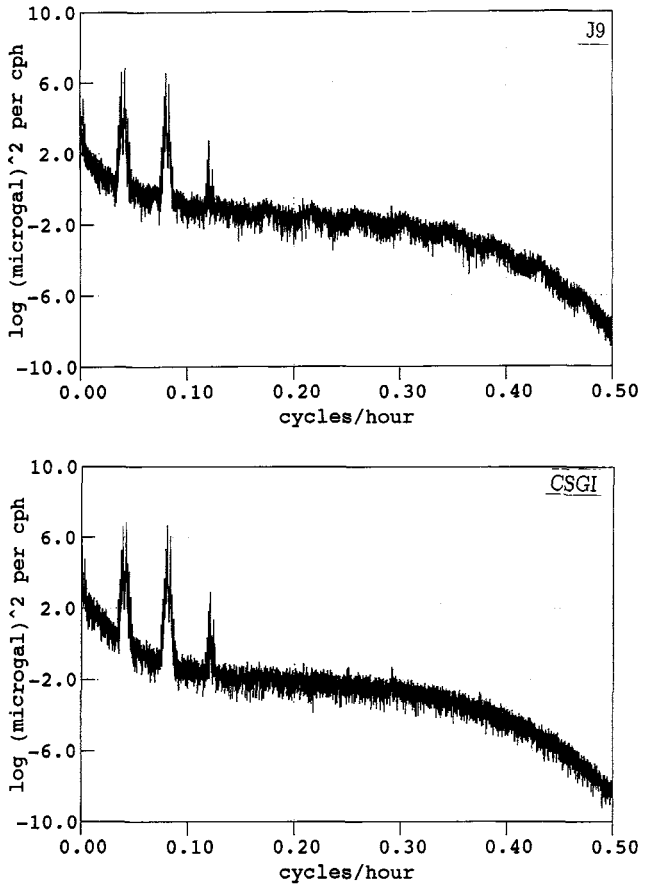

Figure 3. Power spectral density (expressed in μgal^2 per cph) of the 1 hr gravity signals. The high-frequency behaviour shows the attenuation caused by the decimation filter. This spectrum has been smoothed with an 11-point Parzen spectral window.

predominantly low frequency. The peak shortly to the left of 0.3 cph present in both spectra is a solar frequency and corresponds to the seventh harmonic of the solar tide S_1 known to be fairly large in the world atmospheric pressure (see also Fig. 6). The regular humps (periodicities in the spectrum), which can be seen in the Strasbourg PSD, are not due to any non-linearity or windowing effects but are caused entirely by instrumental disturbances; when we correct the time signal shown in Fig. 2 (the one that leads to the PSD with humps) for major spikes and offsets (typically a few μgal in amplitude), the humps appear then in the PSD of the correcting function and, consequently, disappear in the PSD of the corrected hourly gravity signal. For the same reason they do not appear in the PSD of the Strasbourg gravity residuals shown in Fig. 10 (obtained after a least-squares fit procedure applied to the corrected gravity which is explained later). A similar investigation on the Cantley data shows that humps with smaller amplitude and higher frequency are also present but they are much less obvious.

As already mentioned, the total power of the Cantley raw gravity is larger than that of Strasbourg essentially because of the large drift contribution; this can be seen in bands 1 and 2 in Table 1, where the statistics of the PSD are shown. In comparison, the signal level in the intertidal (4, 6, 8) and subtidal bands (10, 11) is smaller for CSGI than for J9. The rms normalized amplitude (μgal) is defined to give the true amplitude of a purely harmonic signal. Consider, for instance, the frequency band 10 (periods just below the fourth diurnal tidal band) for Strasbourg where the rms amplitude is 2.35 ngal. Within this band, any harmonic signal of say 5 ngal would appear at twice the rms value and hence be visible above the noise level in the amplitude spectrum. The mean PSD is expressed in μgal^2 per cph and is simply the arithmetic mean of the PSD values per band. The integrated PSD is the power in μgal^2 integrated for each frequency band (to get the total power present in the signal, one has to multiply the value in every band by a factor 2 because the PSD is symmetrical for negative frequencies). Finally the equivalent time standard deviation (sd) is in μgal and corresponds to a band-limited white noise signal the PSD of which would be constant in the selected frequency band (for such a signal, the power is simply sd^2).

It must be noted that the total power computed in Table 1 is slightly lower than the true observed power because of the effect of the cosine bell taper. An analytical calculation shows that the ratio

$$\int_0^T \omega_{cb}^2(t)\,dt \Big/ \int_0^T \omega_b^2(t)\,dt,$$

where ω_{cb} is the cosine bell taper and ω_b the box-car taper, is 0.9375 for a 10 per cent length of the taper with respect to the total length T. This means that the power estimates of the tapered data have to be multiplied by a factor $1/0.9375 = 1.066$. The corresponding standard deviations (as well as the rms normalized amplitudes) should then be corrected by $(1.066)^{0.5} = 1.0326$. In various tests, we have retrieved these analytical values by comparing the spectral statistics of tapered random white noise signals versus untapered ones.

Barometric pressure

The local barometric pressure is usually recorded less often than the gravity (e.g. every 10 s in Cantley and every 20 s in Strasbourg) and is first decimated by low-pass filtering (these filters are different from those applied to gravity) to a 5 min sampling rate. The same decimation filter as the one applied to the 5 min gravity samples provides hourly values of air pressure, for both data sets in this pre-processing. The time fluctuations of the hourly values of the atmospheric local pressure are given in Fig. 4 (the reference level in both records is arbitrary). Although the range of pressure variations is comparable in both records with standard deviations of the order of 8 mbar, as indicated by the histograms in Fig. 5, we see that the Cantley pressure fluctuates more rapidly than in Strasbourg, reflecting the different characteristics of the weather systems. Atmospheric pressure fronts reaching several 10s of mbar in a short time span appear on both records. Although the pressure histograms are more Gaussian than those for gravity, there is still an excess of kurtosis, as well as a (small) negative skewness. The PSD of the pressure signals are given, again on a logarithmic scale, in Fig. 6 (same smoothing as for the gravity PSD) and clearly show the power-law decrease of the atmospheric pressure with frequency; the tail of the spectra is, as before, the

Table 1. Statistics on the spectral content of the raw observed gravity signals. The frequency bands 3, 5, 7, 9 correspond to the diurnal, semi-diurnal, ter-diurnal and quarter-diurnal tidal bands. The top part is relative to Strasbourg (J9), the bottom part to Cantley (CSGI). The rms normalized amplitude is expressed in μgal. The mean power spectral density (PSD) is in μgal^2 per cph. The power (integrated PSD) is in μgal^2. The equivalent time standard deviation is in μgal.

(J9)

band #	width cycles/hour	rms normalised amplitude	mean PSD	integrated PSD	equivalent time standard deviation
1	.000- .014	1.0828	5135.3	72.013	71.658
2	.014- .033	.43454E-01	8.2703	.15724	2.8758
3(D)	.033- .047	4.1632	75914.	1063.4	275.53
4	.047- .075	.13577E-01	.80732	.22617E-01	.89852
5(S)	.075- .089	2.6979	31881.	447.07	178.55
6	.089- .117	.59840E-02	.15684	.43938E-02	.39603
7(T)	.117- .131	.29071E-01	3.7015	.51849E-01	1.9239
8	.131- .158	.38611E-02	.65298E-01	.17646E-02	.25554
9(Q)	.158- .172	.33849E-02	.50182E-01	.70294E-03	.22402
10	.172- .333	.23454E-02	.24095E-01	.38796E-02	.15523
11	.333- .500	.43150E-03	.81552E-03	.13621E-03	.28557E-01
12	.000- .500	.85009	3165.2	1582.7	56.261

(CSGI)

band #	width cycles/hour	rms normalised amplitude	mean PSD	integrated PSD	equivalent time standard deviation
1	.000- .014	9.0611	.35961E+06	5042.8	599.68
2	.014- .033	.69537E-01	21.179	.40266	4.6021
3(D)	.033- .047	4.2683	79794.	1117.7	282.48
4	.047- .075	.10154E-01	.45157	.12651E-01	.67200
5(S)	.075- .089	3.0704	41292.	579.04	203.21
6	.089- .117	.32734E-02	.46933E-01	.13149E-02	.21664
7(T)	.117- .131	.35001E-01	5.3659	.75164E-01	2.3164
8	.131- .158	.19614E-02	.16849E-01	.45533E-03	.12981
9(Q)	.158- .172	.18713E-02	.15337E-01	.21484E-03	.12385
10	.172- .333	.12120E-02	.64337E-02	.10359E-02	.80211E-01
11	.333- .500	.21611E-03	.20455E-03	.34165E-04	.14302E-01
12	.000- .500	1.7543	13479.	6740.0	116.10

consequence of the decimation filter. On top of this signal, the harmonic components of the thermal tide from S_1 to S_9 are clearly visible on both stations (see also Florsch *et al.* 1991), as expected from the known global distribution of this tide in the atmosphere (Haurwitz & Cowley 1973). Although the gravity PSD has a shape similar to the pressure PSD, the level of the gravity PSD is far larger than that which would be induced from the pressure PSD, assuming a local admittance of $-0.3\,\mu$gal mbar^{-1} when correcting the gravity for the effect of atmospheric loading (e.g. Warburton & Goodkind 1977); this means that the gravity spectrum can be only partly attributed to local pressure fluctuations. Other known contributions come from regional or even global atmospheric loading (Van Dam & Wahr 1987; Merriam 1992a), instrumental effects and local site disturbances.

Gravity residual signal

In the next numerical step we have performed, for each station, a traditional tidal fitting procedure of the raw gravity signal with respect to a theoretical tidal potential, introducing a low-order polynomial for the drift behaviour and taking into account the local pressure as an additional channel. We used a standard tidal package called HYCON (hybrid least-squares frequency domain convolution) (Schüller 1986) based on the CTE tidal development (Cartwright & Tayler 1971; Cartwright & Edden 1973) with 505 waves, and introduced a parabolic (order two) function for the drift, as well as a single coefficient for the atmospheric pressure admittance. We did some tests using a three-term admittance function which allows for a frequency dependence of the gravity response to the pressure, but the results were unsatisfactory due to non-stationarity of the low-frequency pressure variations. Recent tidal developments are now available with more waves than the CTE expansion (Tamura 1987; Xi Quiwen 1987, 1989; Merriam 1992b) and are known to be better than the CTE expansion, as shown by Wenzel and Zürn (1990) and Hinderer, Crossley & Florsch (1991a). In this comparative study where we concentrate on gravity residuals outside the tidal bands, we accept the limitations of the CTE potential and do not

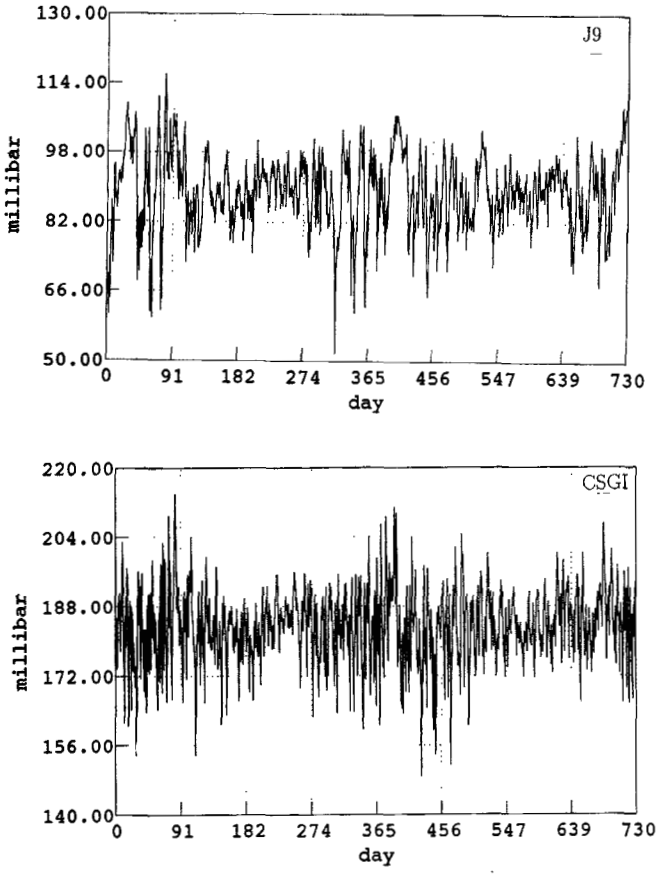

Figure 4. Time fluctuations of the 1 hr local atmospheric pressure signals.

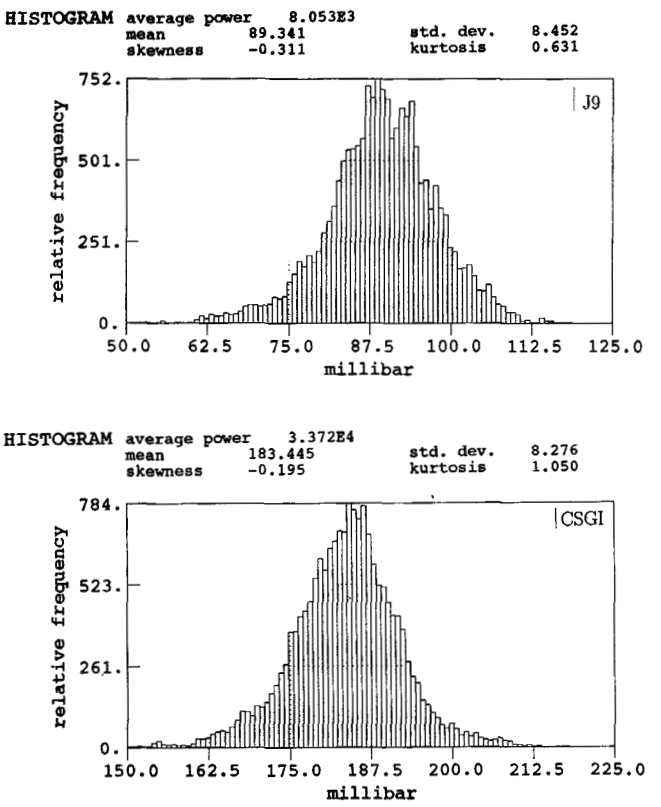

Figure 5. Histograms of the pressure signals shown in Fig. 4.

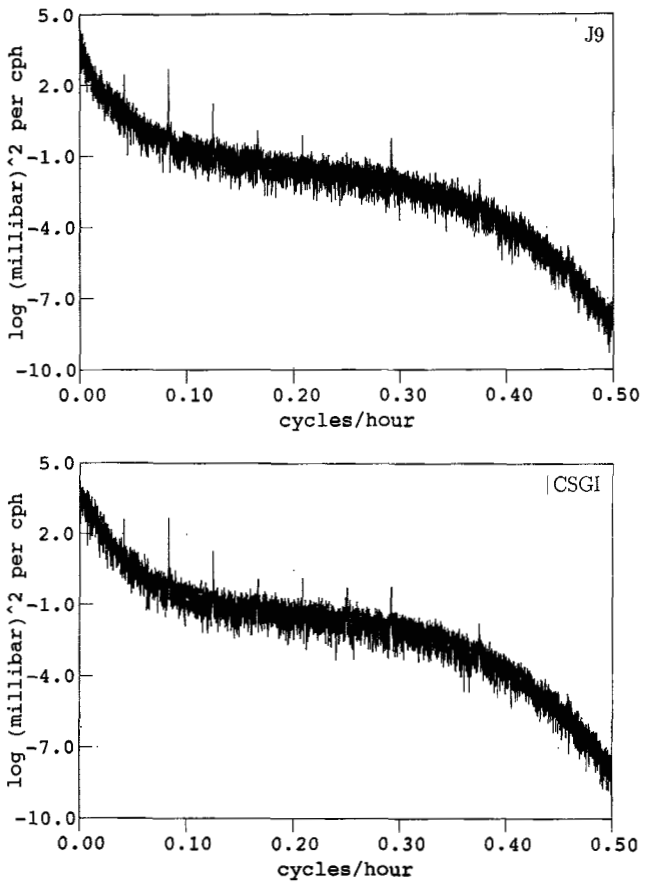

Figure 6. Power spectral density (expressed in mbar^2 per cph) of the 1 hr pressure signals. The high-frequency behaviour shows the attenuation caused by the decimation filter. This spectrum has been smoothed with an 11-point Parzen spectral window.

Table 2. Polynomial drift coefficients and local barometric admittance. a_1 is the linear term expressed in μgal which multiplies (t/T), where t is the elapsed time from the beginning of the common observing period and T the full two-year length. a_2 is the quadratic term again in μgal which multiplies $(t/T)^2$. b is the local atmospheric admittance expressed in μgal mbar^{-1}. The first two lines are for the unfiltered gravity and pressure signals (low frequencies included) and the last two lines for high-passed (periods shorter than three days) and despiked signals.

	a_1 (μgal)	a_2 (μgal)	b ($\mu gal/mbar$)
J9	8.32 ± 0.19	10.57 ± 0.19	- 0.247 ± 0.002
CSGI	- 428.35 ± 0.11	48.10 ± 0.11	- 0.281 ± 0.001
J9 (HP)	0.012 ± 0.017	- 0.017 ± 0.017	- 0.330 ± 0.001
CSGI (HP)	- 0.015 ± 0.015	0.018 ± 0.014	- 0.322 ± 0.001

further investigate the use of more precise tidal potentials. The gravity residual signal is the result of subtracting, from the raw gravity, the HYCON fit of tides, drift and a local pressure correction. Assuming linearity, the effect of a better tidal potential on the residuals should have a minimal effect outside the tidal bands, but will improve the determination of the gravimetric amplitude and phase factors (δ_i, κ_i) of the tidal wave groups that appear in eq. (2); the number of such factors that can be separated depends on the length of data available.

The polynomial coefficients of the drift and the barometric admittance given by the least-squares inversion are listed in Table 2. As indicated above, a more detailed analysis of the tidal content in both records will be presented elsewhere, so we refrain from giving here the gravimetric factors resulting from the HYCON fit.

As expected, the CSGI drift term is well represented by a large linear drift towards negative gravity values, as can be seen on the so-called tide-free signal (raw gravity—fitted tides) plotted on the bottom of Fig. 7; on the other hand, the drift component in J9 is much smaller and increases gravity with time (Fig. 7, top). One reason for this difference is that the Strasbourg instrument was installed almost three years before the beginning of this common observing period (February 1987), so its drift rate has decreased considerably from a much larger initial drift rate. In contrast, the Cantley gravimeter was installed only a few months before the starting date of this study; however this

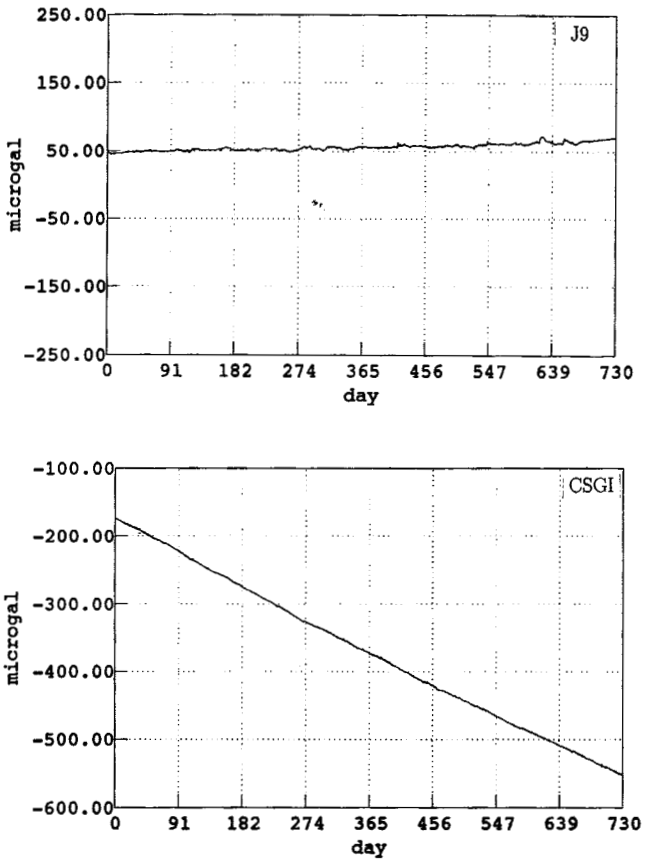

Figure 7. Time fluctuations of the tide-free gravity signals after a least-squares fit to lunisolar tides, drift and local atmospheric pressure.

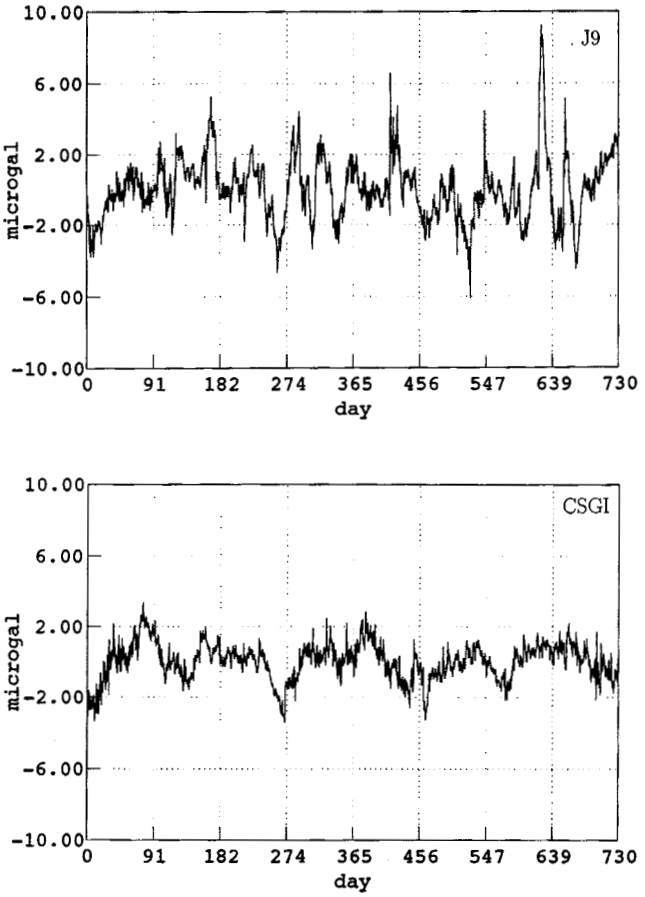

Figure 8. Time fluctuations of the gravity residual signals after a least-squares fit to lunisolar tides, drift and local atmospheric pressure.

large linear drift is due primarily to the unusual instrumental characteristics of this instrument. The tide-free signal contains, in addition to the polynomial drift, all unmodelled physical effects, as well as the pressure-induced gravity.

The signals plotted in Fig. 8 are the gravity residuals which have a much smaller range than the tide-free signals. It is worth noting that, because an annual tidal wave of gravitational origin (S_a) was included in the tidal potential used in HYCON, any geophysical signal of annual period has been removed by the fitting procedure. In our case, annual signals of several μgal amplitude (with large apparent delta factors and large phase shifts with respect to the annual tide S_a) were found and might correspond to annual gravity perturbations of global geodynamic origin (see e.g. Hinderer & Legros 1991; Hinderer *et al.* 1991b). This point will be investigated in more detail in the future.

The gravity residuals have zero mean and a range of a few μgal, as shown by the histograms in Fig. 9. As compared with the raw hourly data, the power has been reduced by about 10^4 (approximately 120 in standard deviation) for the Cantley station and about 10^3 for the Strasbourg station (32 in sd). Still visible on both plots are a number of spikes (large sudden gravity excursions) and offsets. Although the raw gravity sd was larger for CSGI than for J9 (due mainly to the large drift of the Canadian instrument), this is no longer true for the residual gravity as the CSGI sd is approximately

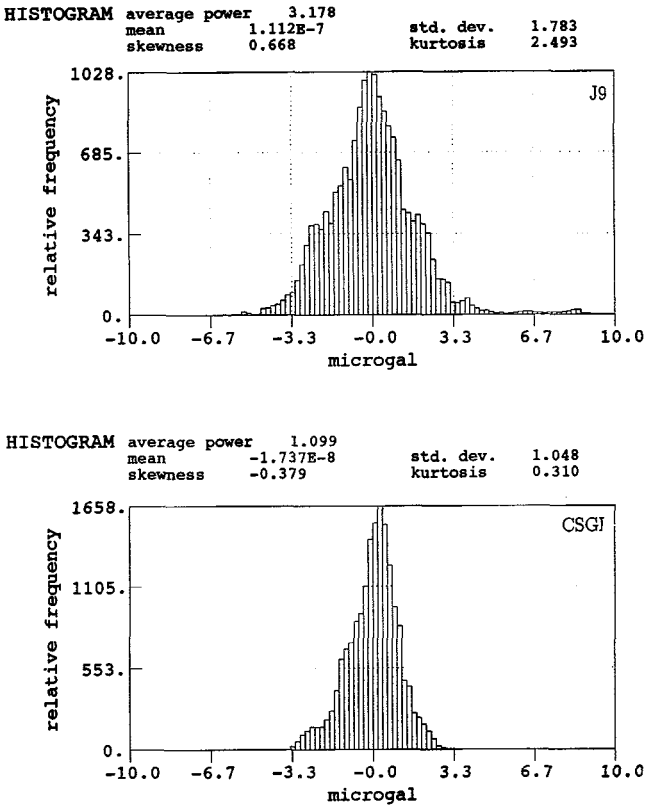

Figure 9. Histograms of the residual gravity signals shown in Fig. 8.

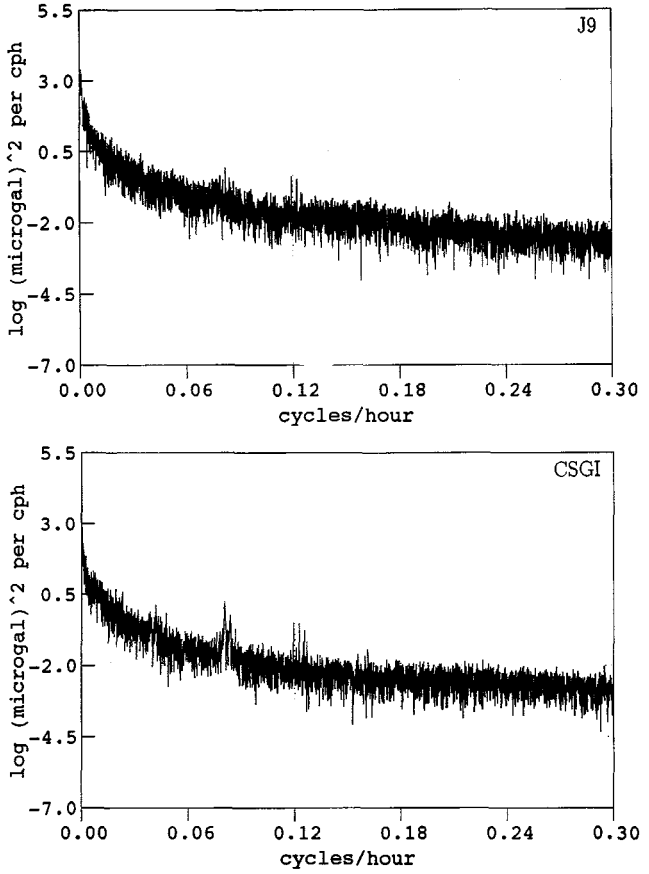

Figure 10. Power spectral density (expressed in μgal^2 per cph) of the residual gravity signals shown in Fig. 8. This spectrum has been smoothed with an 11-point Parzen spectral window.

0.6 of the J9 sd. This important result demonstrates that the removal of a well-defined instrument drift is not a major obstacle in reaching low-amplitude gravity residuals. The PSD of the gravity residuals (smoothed as before) are shown in Fig. 10, omitting frequencies higher than 0.3 cph which are attenuated by the decimation filter. Most of the tidal energy has disappeared and there is still a slight decrease of the residual signal with frequency (power-law type) in both stations. The spectral content of these signals is given in Table 3 for different tidal and non-tidal frequency bands. Note that the residual power is dominated at both stations by low-frequency contributions (especially band 1) and decreases with frequency throughout the spectrum. Most significantly, the power is lower for CSGI than for J9, for every frequency band (except semi-diurnal band 5, possibly because of a larger oceanic loading effect in Canada), particularly for the low frequencies.

We have used gravity residuals (not shown) from an initial least-squares fit to locate in time remaining disturbances and to correct the raw gravity within the new gaps with the same synthetic local tide as in the pre-processing step (on 5 min samples). A new least-squares procedure was then performed that provided the new gravity residuals shown on Fig. 8. It must be mentioned that large spikes or offsets (typically a few 10s of μgal) can readily be detected by a careful visual examination of the gravity records even when the low-frequency contribution is present, but it is much more delicate and arbitrary to remove smaller perturbations (typically a few μgal) only shown by the gravity residual signal after the first least-squares fit. We found a reduction of the gravity noise level in all the frequency bands with respect to the initial residual gravity (the one obtained after the initial pre-processing). This is not surprising because the removed time signal is made of a succession of minor spikes and offsets the PSD of which has itself a power-law frequency dependence.

HIGH-PASS FILTERING AND AUTOMATIC DESPIKING

In this section, we investigate the content of the gravity signal for periods shorter than a day by first removing the low frequencies in the hourly data. The high-pass filter used has 361 coefficients (more than two weeks long) and a cut-off period of three days; its spectral response is the lower plot of Fig. 1.

One of the motivations to first high-pass (HP) the 1 hr gravity (and pressure) before the fitting procedure is to reduce the effect of various low-frequency contributions which cannot be well accounted for. In particular, the long-period atmospheric loading cannot be well modelled by the use of only a single local admittance because regional and global pressure changes are important and non-stationary, as shown recently by Merriam (1992a). Moreover, the long-term drift will also be strongly attenuated by the HP filter, as shown by Table 2. This table also includes the barometric admittance found from the

Table 3. Statistics on the spectral content of the residual gravity signals after a least-squares fit of unfiltered gravity to tides, drift and local barometric pressure.

(J9)

band #	width cycles/hour	rms normalised amplitude	mean PSD	integrated PSD	equivalent time standard deviation
1	.000- .014	.15086	99.681	1.3978	9.9841
2	.014- .033	.18029E-01	1.4237	.27068E-01	1.1932
3(D)	.033- .047	.84082E-02	.30965	.43375E-02	.55647
4	.047- .075	.53570E-02	.12570	.35214E-02	.35454
5(S)	.075- .089	.44605E-02	.87144E-01	.12220E-02	.29520
6	.089- .117	.25484E-02	.28445E-01	.79690E-03	.16866
7(T)	.117- .131	.24749E-02	.26827E-01	.37579E-03	.16379
8	.131- .158	.20324E-02	.18092E-01	.48892E-03	.13451
9(Q)	.158- .172	.18817E-02	.15508E-01	.21723E-03	.12453
10	.172- .333	.10225E-02	.45790E-02	.73727E-03	.67669E-01
11	.333- .500	.18948E-03	.15724E-03	.26264E-04	.12540E-01
12	.000- .500	.25610E-01	2.8727	1.4364	1.6949

(CSGI)

band #	width cycles/hour	rms normalised amplitude	mean PSD	integrated PSD	equivalent time standard deviation
1	.000- .014	.85306E-01	31.944	.44795	5.6436
2	.014- .033	.12247E-01	.65689	.12489E-01	.81049
3(D)	.033- .047	.63804E-02	.17831	.24977E-02	.42227
4	.047- .075	.32673E-02	.46758E-01	.13100E-02	.21624
5(S)	.075- .089	.52137E-02	.11906	.16696E-02	.34505
6	.089- .117	.16916E-02	.12533E-01	.35111E-03	.11195
7(T)	.117- .131	.18029E-02	.14237E-01	.19943E-03	.11932
8	.131- .158	.11167E-02	.54618E-02	.14760E-03	.73904E-01
9(Q)	.158- .172	.98531E-03	.42522E-02	.59564E-04	.65210E-01
10	.172- .333	.74084E-03	.24039E-02	.38706E-03	.49030E-01
11	.333- .500	.14642E-03	.93894E-04	.15683E-04	.96900E-02
12	.000- .500	.14588E-01	.93405	.46704	.96510

regression between the HP local pressure and gravity signals. The HP admittances are larger than those of the unfiltered data and closer to the theoretical value of $-0.356\ \mu$gal mbar^{-1} proposed by Merriam (1992a). Because higher frequency pressure fluctuations occur on a local scale, the unfiltered admittances, which combine local and regional effects, are more station-dependent than the HP admittances and this could explain the larger discrepancy between raw admittance values.

It is evident that spikes remain in the HP gravity residuals (Fig. 11). These transient signals, either man-made (instrumental maintenance, helium transfer) or caused by earthquakes, are removed by an automatic procedure that has a threshold level of three times the sd of the residuals (respectively, $0.5\ \mu$gal for CSGI and $0.7\ \mu$gal for J9), as given by the histograms of the HP residuals (Fig. 12). The correcting (despiking) function is shown in Figs 13(a) and (c) for J9 and CSGI, respectively. This signal is then subtracted from the HP hourly gravity signal prior to a new HYCON fit. Figs 13(b) and (d) show the HP gravity residuals for J9 and CSGI, respectively, obtained from this new fit.

Our final pair of PSD is shown in Fig. 14 in the unsmoothed form and in Fig. 15 using the same amount of smoothing as in the previous spectra. The related statistics are given in Table 4. The HP filter clearly reduces long-period power and, as previously, we omit the high frequencies ($\geq$0.3 cph) because of the decimation filter. Comparing Tables 3 and 4, we see that, aside from frequency bands 1 and 2 (which are heavily filtered), the overall power has been reduced everywhere except in the highest frequency band (11). Again the gravity noise level is slightly lower for the Canadian station compared with the French one. Fig. 16 shows the normalized amplitude spectra in the range 0.10–0.30 cph. Tidal residual signals are left with amplitudes less than 10 ngal in the ter-diurnal band and less than 5 ngal in the quarter-diurnal band. The gravity level is a few ngal in the intertidal bands and slightly less than 1 ngal in the subtidal band 10. It appears from Table 4

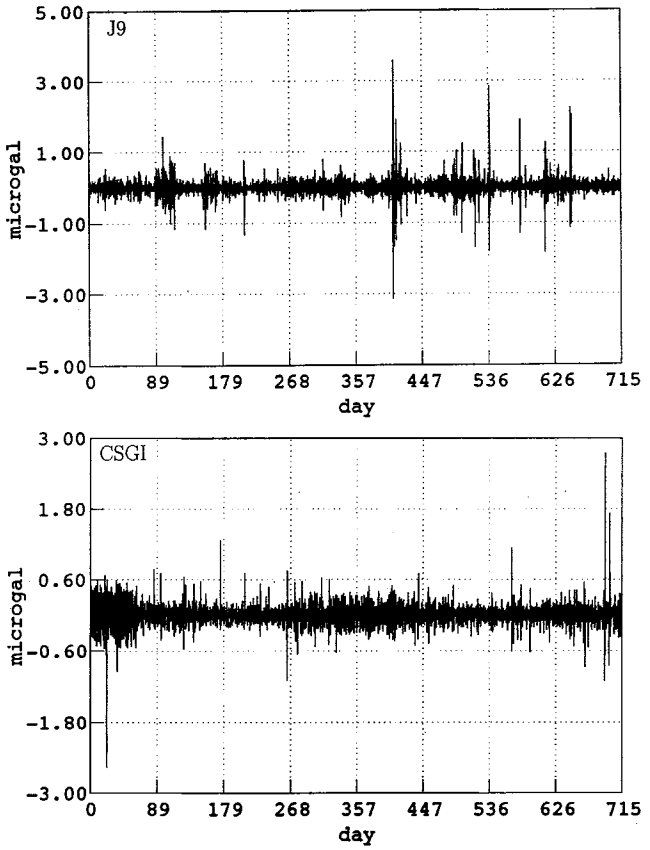

Figure 11. Time fluctuations of the residual gravity signals after a least-squares fit to lunisolar tides, drift and local atmospheric pressure for the high-passed gravity and pressure signals (cut-off period of three days).

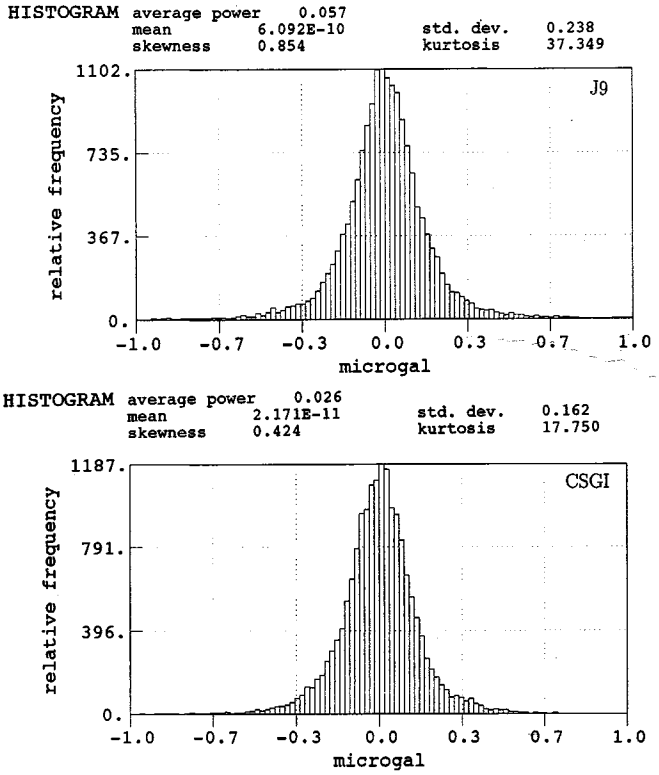

Figure 12. Histograms of the residual gravity signals shown in Fig. 11.

(especially for the less noisy CSGI station) that the ngal level is attained in the subtidal band (for periods between 6 and 3 hr), at the limit below which periodical geophysical signals from the Earth's deep interior may be present (see e.g. Hinderer & Crossley 1993). The ngal level was shown by a recent study dealing with the seismic excitation of core modes (Crossley, Hinderer & Legros 1991) to be the detectability limit of surface gravity effects related to core dynamics.

In global geodynamics we expect to see gravity contributions have a world-wide spatial extension and an obvious way to investigate common features in both records is to compute the cross-spectral analysis of our gravity signals. We have therefore computed the cross-PSD estimates (defined as the magnitude of the product of the two complex Fourier transforms relative to each individual record) from our final pair of HP gravity residuals. As expected from a stacking procedure, we found that the noise level of the unsmoothed cross-PSD (not shown) is somewhere in-between the individual levels for each station shown in Fig. 14. The same smoothing procedure as before (11-point Parzen window) was applied to the complex cross-spectrum and leads to the smoothed cross-PSD shown at the top of Fig. 17. The corresponding normalized cross-amplitude spectrum is shown at the bottom of Fig. 17. Residual tidal lines, which are expected to be present in both records, are reinforced by the method and emerge clearly from the ambient noise which tends to decrease because of the smoothing effect on incoherent random signals. The mean level of the smoothed PSD is then further decreased and reaches a value of about 1.3×10^{-3} μgal^2 per cph in the subtidal band 10 (0.17–0.33 cph), as indicated by Table 5. This level appears to be substantially lower (by a factor close to 5 in PSD) than the one derived from the product spectrum of four European SCG records (Smylie 1992; Smylie *et al.* 1993). However, one has to keep in mind that these European data sets and the ones discussed here are for different time intervals and, even more importantly, were processed in many different ways (disturbance corrections, least-squares fit, spectral analysis). From synthetic data calibration, we found that a pure harmonic signal of 1 ngal amplitude injected at the same frequency in each of our two records (in the hourly raw gravity signals) would appear at a level of 1.6×10^{-3} μgal^2 per cph in the cross-spectrum and therefore would be marginally above the mean noise level and virtually undetectable in the subtidal band of the cross-spectrum shown in Fig. 17. Remembering that the detectability limit of surface gravity effects related to core dynamics is indeed 1 ngal, we see that a clear identification of such effects is a very difficult task even in a stack of good quality SCG data.

CONCLUSIONS

We have presented for the first time a comparison of data from two well-separated superconducting gravimeters over a common observing period of two years. These data have been treated following exactly the same numerical procedure (decimation, filtering, least-squares fit) for each station. The comparison of the raw gravity data (low frequencies included) shows that the drift behaviour of the two instruments is totally different, the Canadian station

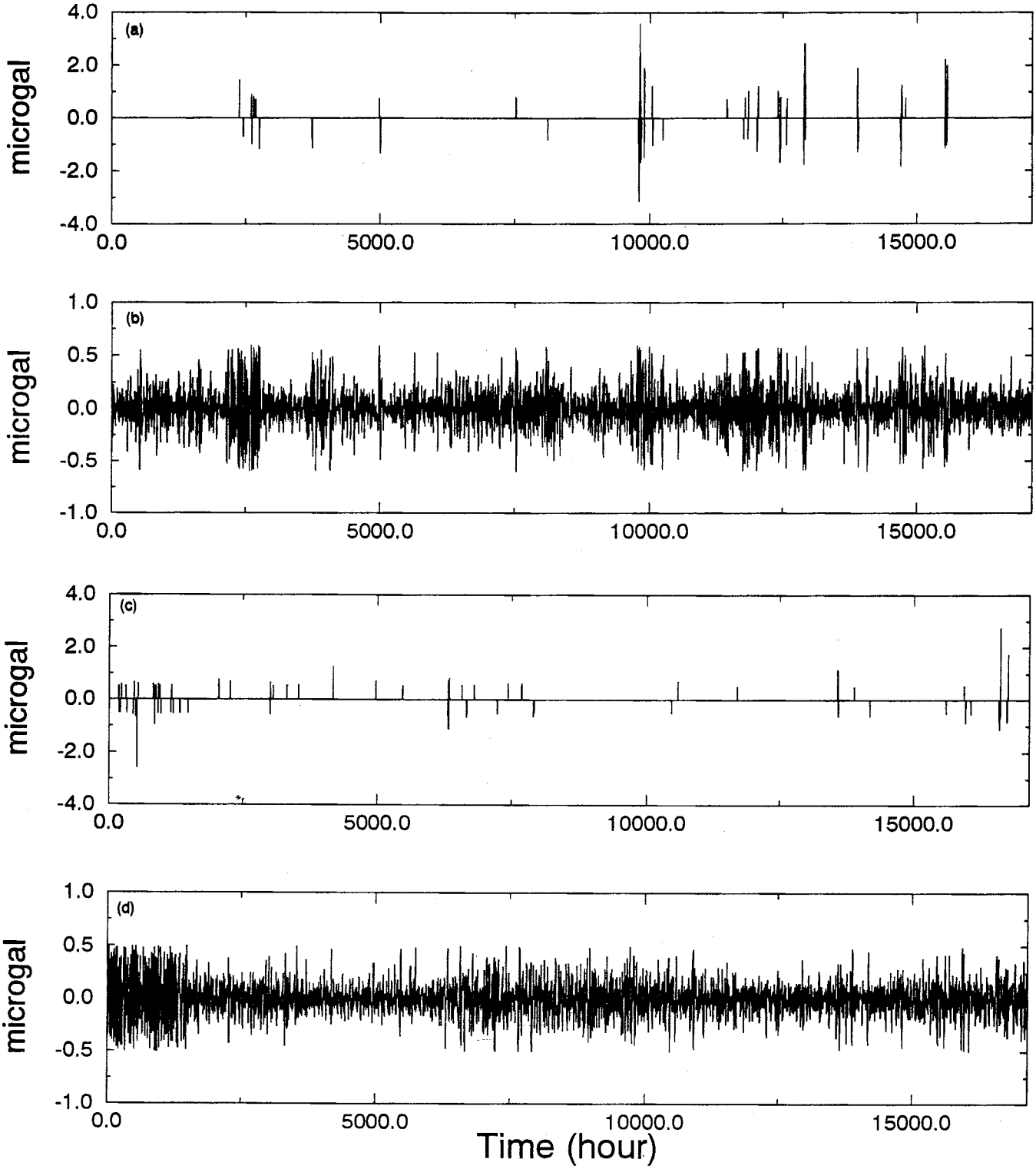

Figure 13. Automatic despiking procedure applied to the high-passed gravity data. (a) and (c) are the correcting functions for J9 and CSGI, respectively, and are a succession of spikes exceeding 3 sd of the residual signal shown in Fig. 11 (0.7 μgal for J9 and 0.5 μgal for CSGI). (b) and (d) are the new (high-passed) residual gravity signals for J9 and CSGI, respectively, after subtracting the signals (a) and (c) from the high-passed 1 hr gravity and refitting the tides, drift and local atmospheric pressure.

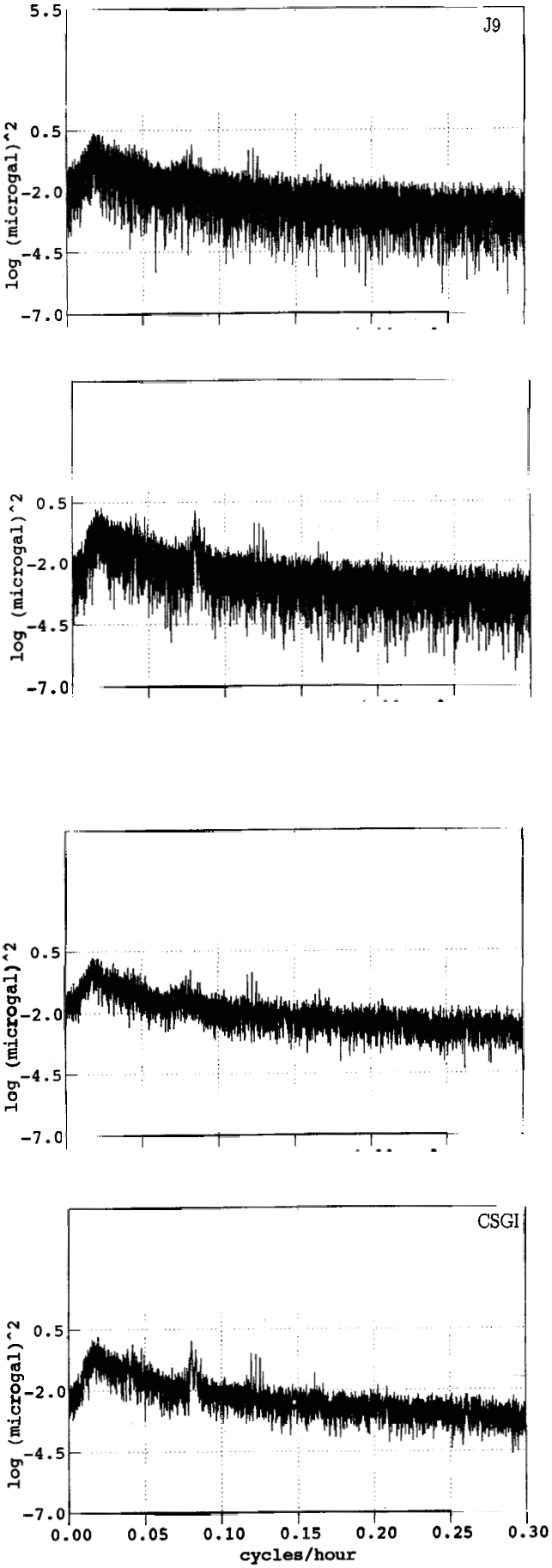

Figure 15. Smoothed version (11-point Parzen spectral window) of the power spectral density shown in Fig. 14.

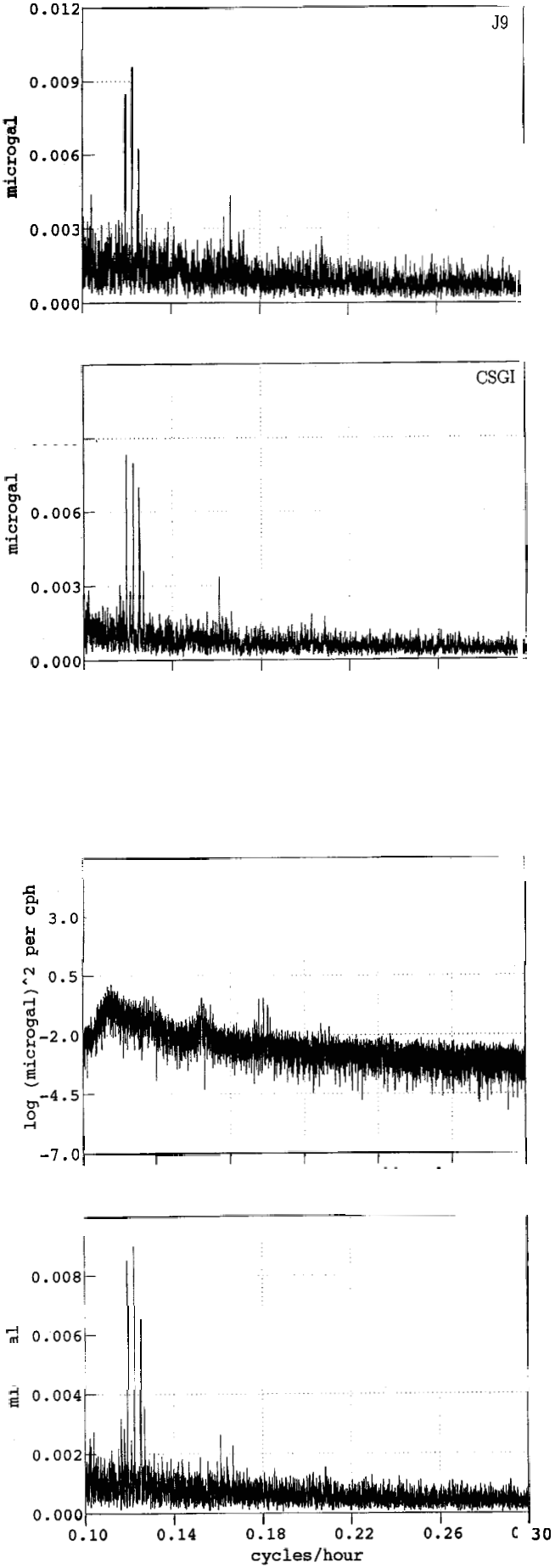

Figure 17. Cross-spectral estimates of the residual gravity signals shown in Fig. 13. The top curve is the cross PSD and the bottom the normalized cross-amplitude. We used the same smoothing amount as before (11-point Parzen spectral window) applied to the complex cross-spectral values.

Table 4. Statistics on the spectral content of the residual gravity signals after a least-squares fit of high-passed (periods shorter than three days) and despiked gravity to tides, drift and local barometric pressure.

(J9)

band #	width cycles/hour	rms normalised amplitude	mean PSD	integrated PSD	equivalent time standard deviation
1	.000- .014	.40049E-02	.68808E-01	.96490E-03	.26231
2	.014- .033	.88340E-02	.33479	.63652E-02	.57861
3(D)	.033- .047	.52727E-02	.11927	.16707E-02	.34535
4	.047- .075	.31780E-02	.43327E-01	.12138E-02	.20815
5(S)	.075- .089	.32409E-02	.45060E-01	.63188E-03	.21227
6	.089- .117	.18130E-02	.14101E-01	.39505E-03	.11875
7(T)	.117- .131	.20332E-02	.17734E-01	.24842E-03	.13317
8	.131- .158	.13955E-02	.83549E-02	.22578E-03	.91406E-01
9(Q)	.158- .172	.14105E-02	.85349E-02	.11956E-03	.92385E-01
10	.172- .333	.87850E-03	.33108E-02	.53308E-03	.57540E-01
11	.333- .500	.50155E-03	.10791E-02	.18024E-03	.32850E-01
12	.000- .500	.24181E-02	.25083E-01	.12542E-01	.15838

(CSGI)

band #	width cycles/hour	rms normalised amplitude	mean PSD	integrated PSD	equivalent time standard deviation
1	.000- .014	.34046E-02	.49727E-01	.69732E-03	.22300
2	.014- .033	.70499E-02	.21321	.40538E-02	.46175
3(D)	.033- .047	.47927E-02	.98542E-01	.13803E-02	.31392
4	.047- .075	.23944E-02	.24596E-01	.68906E-03	.15683
5(S)	.075- .089	.42578E-02	.77773E-01	.10906E-02	.27888
6	.089- .117	.13276E-02	.75611E-02	.21183E-03	.86955E-01
7(T)	.117- .131	.17382E-02	.12961E-01	.18156E-03	.11385
8	.131- .158	.92881E-03	.37009E-02	.10001E-03	.60835E-01
9(Q)	.158- .172	.88731E-03	.33775E-02	.47312E-04	.58117E-01
10	.172- .333	.57505E-03	.14186E-02	.22842E-03	.37665E-01
11	.333- .500	.32597E-03	.45586E-03	.76139E-04	.21351E-01
12	.000- .500	.20193E-02	.17493E-01	.87470E-02	.13226

Table 5. Statistics on the smoothed (11-point Parzen spectral window) cross-spectral estimates of the high-passed and despiked gravity residuals.

band #	width cycles/hour	rms normalised amplitude	mean PSD	integrated PSD	equivalent time standard deviation
1	.000- .014	.29035E-02	.36164E-01	.50713E-03	.19017
2	.014- .033	.63443E-02	.17267	.32830E-02	.41554
3(D)	.033- .047	.40019E-02	.68705E-01	.96241E-03	.26212
4	.047- .075	.22491E-02	.21701E-01	.60797E-03	.14731
5(S)	.075- .089	.27464E-02	.32357E-01	.45375E-03	.17988
6	.089- .117	.12110E-02	.62912E-02	.17625E-03	.79318E-01
7(T)	.117- .131	.16686E-02	.11944E-01	.16730E-03	.10929
8	.131- .158	.88994E-03	.33976E-02	.91815E-04	.58289E-01
9(Q)	.158- .172	.85993E-03	.31723E-02	.44437E-04	.56324E-01
10	.172- .333	.55294E-03	.13116E-02	.21119E-03	.36217E-01
11	.333- .500	.31017E-03	.41273E-03	.68936E-04	.20316E-01
12	.000- .500	.17497E-02	.13134E-01	.65673E-02	.11460

exhibiting a large almost linear drift towards negative gravity, while the French station drift is much smaller towards positive gravity. The power levels found in the gravity residual signal (the result of subtracting a fit to tides), drift and local pressure admittance, are comparable, though the Cantley station shows a lower level in almost every frequency band compared with Strasbourg. The statistics of the spectral content of the gravity residual signal permits an objective comparison of the two data sets. After a high-pass filtering procedure was applied to the raw pressure and gravity signals, the power level in the residual gravity signal was found to be reduced in all bands (tidal and non-tidal) with respect to the unfiltered residual signal. To remove obvious spikes left in the high-passed residuals, we applied an automatic detection procedure with a threshold equal to three times the standard deviation of the uncorrected gravity signal. The results lead to an effective reduction of the power levels for all frequencies at both stations. The cross-spectral estimates we obtain from these two individual residual records finally show a further reduction of the power level because of the smoothing effect on incoherent random signals. A normalized amplitude cross-spectrum indicates a level of several ngal in the tidal and intertidal bands, and less than 1 ngal in the subtidal band in the 6–3 hr period.

ACKNOWLEDGMENTS

D. Crossley wishes to acknowledge funding through Canadian NSERC Operating and Infrastructure grants. J. Hinderer would like to thank NSERC for providing an International Research Fellowship during his sabbatical at McGill University. This study has also been supported by INSU–CNRS (France). We would like to thank W. Zürn and L. Mansinha for their comments, criticisms and suggestions on this paper. We also acknowledge numerous interesting discussions with O. Jensen on the content of the gravity signal and the processing methods.

REFERENCES

Aldridge, K. & Lumb, L. I., 1987. Inertial waves identified in the Earth's fluid outer core, *Nature*, **325,** 421–423.

Aldridge, K., Lumb, L. I. & Anderson, G., 1988. Inertial modes in the Earth's fluid outer core, in *Structure and Dynamics of the Earth's Deep Interior, Geophys. Monogr. Ser.*, **46,** 13–21, eds Smylie, D. E. & Hide, R., Am. Geophys. Un., Washington, DC.

Bower, D. R., Liard, J., Crossley, D. & Bastien, R., 1991. Preliminary calibration and drift assessment of the superconducting gravimeter GWR12 through comparison with absolute gravimeter JILA2, in *Proc. ECGS Workshop on 'Non-tidal gravity changes: intercomparison between absolute and superconducting gravimeters'*, Vol. 3, pp. 129–142, Cahiers du Centre Européen de Géodynamique et de Sésmologie, Walferdange, Luxembourg.

Cartwright, D. E. & Edden, A. C., 1973. Corrected tables of tidal harmonics, *Geophys. J. R. astr. Soc.*, **33,** 253–264.

Cartwright, D. E. & Tayler, R. J., 1971. New computations of the tide-generating potential, *Geophys. J. R. astr. Soc.*, **23,** 45–74.

Crossley, D. J., Hinderer, J. & Legros, H., 1991. On the excitation, detection and damping of core modes, *Phys. Earth planet. Inter.*, **68,** 97–116.

Crossley, D. J., Rochester, M. & Peng, Z., 1992. Slichter modes and Love numbers, *Geophys. Res. Lett.*, **19,** 1679–1682.

Dehant, V. & Ducarme, B., 1987. Comparison between the theoretical and observed tidal gravimetric factors, *Phys. Earth planet. Inter.*, **49,** 192–212.

Dehant, V. & Zschau, J., 1989. The effect of mantle inelasticity on tidal gravity: a comparison between the spherical and elliptical Earth model, *Geophys. J.*, **97,** 549–555.

Ducarme, B., Van Ruymbeke, M. & Poitevin, C., 1986. Three years of registration with a superconducting gravimeter at the Royal Observatory of Belgium, in *Proc. 10th Int. Symp. on Earth Tides,* pp. 113–129, ed. Vierra, R., Cons. Sup. Inv. Cient., Madrid.

Florsch, N., Hinderer, J., Crossley, D., Legros, H. & Valette, B., 1991. Preliminary spectral analysis of the residual signal of a superconducting gravimeter for periods shorter than one day, *Phys. Earth planet. Inter.*, **68,** 85–96.

Haurwitz, B. & Cowley, A. D., 1973. The diurnal and semidiurnal barometric oscillations, global distribution and annual variation, *Pageoph.*, **102,** 193–222.

Hinderer, J. & Legros, H., 1989. Elasto-gravitational deformation, relative gravity changes and Earth dynamics, *Geophys. J.*, **97,** 481–495.

Hinderer, J. & Legros, H., 1991. Gravity perturbations of annual period, in *Proc. 11th Int. Symp. on Earth Tides,* pp. 425–429, Kakkuri, J., Schweitzerbart'sche Verlag, Stuttgart.

Hinderer, J. & Crossley, D., 1993. Core Dynamics and surface gravity changes, in *Dynamics of the Earth's Deep Interior and Earth Rotation, Geophys. Monograph Ser.*, **47,** 1–16, eds Le Mouël, J. L., Smylie, D. E. & Herving, T., Am. Geophys. Un., Washington DC.

Hinderer, J., Crossley, D. & Florsch, N., 1991a. Analysis of residual gravity signals using different tidal potentials, *Bull. Inf. Mar. Terr.*, **110,** 7986–8001.

Hinderer, J., Legros, H. & Crossley, D., 1991b. Global Earth dynamics and induced gravity changes, *J. geophys. Res.*, **96,** 20 257–20 265.

Hinderer, J., Florsch, N., Mäkinen, J., Legros, H. & Faller, J. E., 1991c. On the calibration of a superconducting gravimeter using absolute gravity measurements, *Geophys. J. Int.*, **106,** 491–497.

Jenkins, G. & Watts, D., 1969. *Spectral Analysis and its Applications*, Holden-Day, Cambridge.

Mansinha, L., Smylie, D. & Sutherland, B., 1990. Earthquakes and the spectrum of the Brussels superconducting gravimeter data for 1982–1986, *Phys. Earth plant. Inter.*, **61,** 141–148.

Melchior, P., 1983. *The Tides of the Planet Earth,* 2nd edn, Pergamon Press, Oxford.

Melchior, P. & Ducarme, B., 1986. Detection of inertial gravity oscillations in the Earth's core with a superconducting gravimeter at Brussels, *Phys. Earth planet. Inter.*, **42,** 129–134.

Melchior, P., Crossley, D., Dehant, V. & Ducarme, B., 1988. Have inertial waves been identified from the Earth's core, in *Structure and Dynamics of the Earth's Deep Interior, Geophys. Monogr. Ser.*, **46,** 1–12, eds Smylie, D. E. & Hide, R., Am. Geophys. Un., Washington, DC.

Merriam, J. B., 1992a. Atmospheric pressure and gravity, *Geophys. J. Int.*, **109,** 488–500.

Merriam, J. B., 1992b. An ephemeris for gravity tide predictions at the nanogal level, *Geophys. J. Int.*, **108,** 415–422.

Neuberg, J., Hinderer, J. & Zürn, W., 1987. Stacking gravity tide observations in Central Europe for the retrieval of the complex eigenfrequency of the nearly diurnal free wobble, *Geophys. J. R. astr. Soc.*, **91,** 853–868.

Richter, B., 1983. The long-period tides in the Earth tide spectrum, in *Proc. IAG Symp., 18th IUGG General Assembly, Hamburg,* Vol. 1, pp. 204–216.

Richter, B., 1986. The spectrum of a registration with a superconducting gravimeter, in *Proc. 10th Int. Symp. on Earth*

Tides, pp. 131–139, ed. Vierra, R., Cons. Sup. Inv. Cient., Madrid.

Richter, B. & Zürn, W., 1986. Chandler effect and nearly diurnal free wobble as determined from observations with a superconducting gravimeter, in *The Earth's Rotation and Reference Frames for Geodesy and Geodynamics*, pp. 309–315, eds Babcock, A. & Wilkins, G., Kluwer, Dordrecht.

Schüller, K., 1986. Simultaneous tidal and multi-channel input analysis as implemented in the HYCON-method, in *Proc. 10th Int. Symp. on Earth Tides*, pp. 515–520, ed. Vierra, R., Cons. Sup. Inv. Cient., Madrid.

Smylie, D. E., 1992. The inner core translational triplet and the density near Earth's center, *Science*, **255**, 1678–1682.

Smylie, D. E., Xianhua Jiang, Brennan, B. J. & Sato, K., 1992. Numerical calculation of modes of oscillation of the Earth's core, *Geophys. J. Int.*, **108**, 465–490.

Smylie, D. E., Hinderer, J., Richter, B., Ducarme, B. & Mansinha, L., 1993. A comparative analysis of superconducting gravimeter data, in *Dynamics of the Earth's Deep Interior and Earth Rotation, Geophys. Monograph. Ser.* **72**, 91–96, eds Le Mouèl, J. L., Smylie, D. E. & Herving, T., Am. Geophys. Un., Washington, DC.

Tamura, Y., 1987. An harmonic development of the tide generating potential, *Bull. Inf. Mar. Terr.*, **99**, 6813–6855.

Van Dam, T. M. & Wahr, J. M., 1987. Deformations at the Earth's surface due to atmospheric loading: effects on gravity and baseline measurements, *J. geophys. Res.*, **92**, 128–1286.

Warburton, R. J., Beaumont, C. & Goodkind, J. M., 1975. The effect of ocean tide loading on tides of the solid Earth observed with the superconducting gravimeter, *Geophys. J. R. astr. Soc.*, **43**, 707–720.

Warburton, R. J. & Goodkind, J. M., 1977. The influence of barometric pressure variations on gravity, *Geophys. J. R. astr. Soc.*, **48**, 281–292.

Warburton, R. J. & Goodkind, J. M., 1978. Detailed gravity-tide spectrum between one and four cycles per day, *Geophys. J. R. astr. Soc.*, **52**, 117–136.

Wenzel, H. G. & Zürn, W., 1990. Errors of the Cartwright–Tayler–Edden 1973 tidal potential displayed by gravimetric Earth tide observations at BFO Schiltach, *Bull. Inf. Mar. Terr.*, **107**, 755–7574.

Xi Qinwen, 1987. A new complete development of the tide generating potential for the epoch J 2000.0, *Bull. Inf. Mar. Terr.*, **99**, 6786–6812.

Xi Qinwen, 1989. The precision of the development of the tidal generating potential and some explanatory notes, *Bull. Inf. Mar. Terr.*, **105**, 7396–7404.

Zürn, W., Rydelek, P. & Richter, B., 1986. The core-resonance effect in the record from the superconducting gravimeter at Bad Homburg, in *Proc. 10th Int. Symp. on Earth Tides*, pp. 141–147, ed. Vierra, R., Cons. Sup. Inv. Cient., Madrid.

Zürn, W., Richter, B., Rydelek, P. & Neuberg, J., 1987. Comments on detection of inertial gravity oscillations in the Earth's core with a superconducting gravimeter at Brussels, *Phys. Earth planet. Inter.*, **49**, 176–178.